Quantitative study of the rheology of frictional suspensions: Influence of friction coefficient in a large range of viscous numbers

William Chèvremont,[1] Bruno Chareyre,[2,*] and Hugues Bodiguel[1]
[1]*Univ. Grenoble Alpes, CNRS, Grenoble INP, LRP, 38000 Grenoble, France*
[2]*Univ. Grenoble Alpes, CNRS, Grenoble INP, 3SR, 38000 Grenoble, France*

(Received 3 October 2018; published 12 June 2019)

The rheology of dense suspensions is studied by discrete-element method simulation, focusing on the interplay of the solid fraction, confining pressure, shear rate, and viscosity. Using a minimal model based on lubrication and contact forces, we are able to recover experimental results available in the literature, in a very large range of solid fractions. We show that bulk friction is only weakly dependent on contact friction when a normalized shear rate, the so-called viscous number I_v, is kept constant. In contrast, contact friction has a strong influence on the jamming solid fraction ϕ_m. We provide empirical proof that all the rheology could be accounted for using I_v and ϕ/ϕ_m. By separating the contributions of lubrication and contact forces on the total shear stress, it is shown that contacts dominate at a solid fraction above 0.77 of jamming solid fraction. Universal expressions of macroscopic friction and solid fraction as functions of the viscous number are finally offered.

DOI: 10.1103/PhysRevFluids.4.064302

I. INTRODUCTION

Suspensions of solid particles dispersed in a liquid are ubiquitous in nature and in industry. Their rheological properties have been the focus of intense research efforts since they are crucial for many applications to control the flows of these two-phase systems. Despite many experimental, theoretical, and numerical works, a clear consensus has not yet emerged even in the simplest case of monodisperse non-Brownian hard spheres dispersed in a Newtonian viscous liquid, in particular in concentrated regimes. In this particular case, the bulk viscosity is rate independent, and the main question is its dependence on solid fractions.

Purely hydrodynamic approaches are adequate in the dilute regimes and allow predictions of the viscosity increment due to the solid particles [1,2]. However, when the concentration is increased toward close packing, hydrodynamics might not be sufficient to account for the rheological properties of the suspensions, since the typical distance between particles is extremely small. The liquid film which separates two particles induces lubrication forces, which diverge at the approach to contact. This prevents, in principle, solid contact between ideal and perfectly smooth noninteracting particles. However, at these small scales, even a very small particle roughness can be sufficient to invalidate the previous argument. For example, it has been shown that contact between particles is responsible for irreversibility in sheared suspensions [3,4] and peculiar behavior in shear-reversal experiments [5,6]. Solid contact is also believed to be important in addition to repulsive forces to account for non-Newtonian features such as the shear-thickening properties of some suspensions [7–9]. Even for the case of rate-independent viscosity, the fact that the suspension viscosity apparently diverges at a solid fraction ϕ_m also asks for some nonhydrodynamic forces, since ϕ_m typically varies from 0.50 to 0.63, depending on the system under study. It has been proposed that

*bruno.chareyre@grenoble-inp.fr

differences between systems could be due to differences in contact properties, namely differences in contact friction [9,10].

Near jamming, both experimental and numerical approaches face difficulties associated to the divergence of the viscosity with the increase of solid fractions. Available experimental data are scarce close to jamming and are subject to high uncertainties. A noticeable exception is the work of Boyer *et al.* [11] in which normal pressure was imposed, in contrast with the constant volume conditions used in standard rheometry. In their experiment, the imposed pressure P_p is a pressure exerted on the solid particles only, thanks to a grid through which the liquid phase could flow to adjust the suspension solid fraction ϕ (fraction of the total volume occupied by solid particles). They introduced the so-called viscous number I_v, a dimensionless shear rate defined as the ratio of reference viscous stress over confining pressure: $I_v = \eta_f \dot{\gamma}/P_p$, where η_f is the suspending liquid viscosity and $\dot{\gamma}$ is the shear rate. They argue that for non-Brownian particles with only hydrodynamic and contact forces the rheology can be described by I_v alone. This so-called $\mu(I_v)$ rheology is thus completely described by two equations of state, $\mu(I_v)$ and $\phi(I_v)$, where μ is a macroscopic friction coefficient defined as $\mu = \tau/P_p$ and τ is the shear stress. Based on their measurements, Boyer *et al.* [11] proposed phenomenological expressions for these two functions which include contributions from both contact and viscous forces.

The $\mu(I_v)$ rheology been used in the literature to analyze numerical simulations at high solid fraction ($\phi > 0.4$) [12–17]. Results in more dilute regimes are available in Ref. [10]. Although numerical simulations offer great potential to vary independently the contact properties (in our case, friction coefficient, particle roughness, contact stiffness), very few studies focused on how these contact parameters change the whole rheology by varying them systematically [10]. Further, most simulations [12–15] lack validation against experimental data. Some of them [12,17,18] are based on two-dimensional models, which leads to unrealistic solid fractions and fails to account for some phenomena that take place in the vorticity direction, as reported in Ref. [19]. Recently, Marzougui and coworkers proposed a discrete-element method (DEM) approach which incorporates lubrication forces and contact forces [20]. Therein, the long-range hydrodynamic interactions were accounted for by a pore network approach. Herein, we reuse this strategy, which enables realistic simulations from medium to high solid fractions.

In this work, our aim is to study the $\mu(I_v)$ rheology of stiff non-Brownian particles in a wide and extended range of viscous numbers (from semidilute to high solid fraction), and a wide range of microscopic friction coefficient. In the first part, we detail the numerical model and we test the effect of particle roughness and stiffness. Then, we present the simulation results, focusing on $\mu(I_v)$ and $\phi(I_v)$. It is shown that a very good agreement is obtained with the experimental results of Boyer *et al.* [11], assuming a microscopic friction coefficient μ_m of about 0.5 in the experiments. Strikingly, the effective macroscopic friction coefficient $\mu(I_v)$ depends very weakly on μ_m in a large range of parameters. The only exception is for low μ_m and low I_v (close to jamming). Conversely, the influence of μ_m on the jamming solid fraction ϕ_m is strong. We then test the idea that all the rheology could be accounted for using I_v and ϕ/ϕ_m. Finally, by separating the contributions to shear stress of lubrication and contact forces respectively, we show that contact forces dominate at solid fraction above 40%, and we propose universal expressions for $\mu(I_v)$ and $\phi/\phi_m(I_v)$.

II. MODELS AND METHODS

A. Equations of motion

The motion of suspended particles is integrated in time using the discrete-element method (DEM) implemented in Yade-DEM [21]. The method is based on an explicit time integration of the Newton's equations of motion, for each particle,

$$\frac{d}{dt}\begin{pmatrix} m\dot{\mathbf{r}} \\ \mathbf{J\Omega} \end{pmatrix} = \sum \begin{pmatrix} \mathbf{F} \\ \mathbf{T} \end{pmatrix}, \tag{1}$$

where $\mathbf{r}$ is the position of the center of mass of the particle and $\dot{\mathbf{r}}$ is its time derivative, m is the mass, $\mathbf{J}$ is the moment of inertia tensor, $\mathbf{\Omega}$ is the rotational velocity vector, $\mathbf{F}$ denotes forces acting on the body, and $\mathbf{T}$ denots the moments of these forces about $\mathbf{r}$. The total force on a given particle results from pair interactions corresponding to solid contacts and lubrication forces, and seepage forces induced by the differential motion between the solid particles and the suspending fluid. All three types of forces are discussed later.

B. Contact model

The contact forces between particles follow an elastic-frictional contact model, following Cundall and Strack [22]. When a contact is established, two particles of radius a at positions $\mathbf{r}$ and $\mathbf{r}'$ interact by a repulsive force along the contact normal $\mathbf{n}$,

$$\mathbf{F}_n^C = k_n u_n \mathbf{n} \quad \text{if} \quad u_n < 0, \tag{2}$$

$$\text{with } u_n = \|\mathbf{r}' - \mathbf{r}\| - 2a, \quad \mathbf{n} = \frac{\mathbf{r}' - \mathbf{r}}{\|\mathbf{r}' - \mathbf{r}\|}. \tag{3}$$

Here, k_n is the normal stiffness and u_n is the normal displacement, i.e., the change of center-to-center distance relative to the equilibrium configuration. If $u_n \geqslant 0$, there is no contact force.

The shear component of the force is obtained by explicit integration of its time derivative

$$\begin{aligned} \dot{\mathbf{F}}_s^C &= k_s \mathbf{v}_s + \mathbf{\Omega}^C \times \mathbf{F}_s^C, \\ \text{with } \mathbf{v}_s &= \dot{\mathbf{r}}' - \dot{\mathbf{r}} - a(\mathbf{\Omega} + \mathbf{\Omega}') \times \mathbf{n} \\ \text{and } \mathbf{\Omega}^C &= \mathbf{n} \times \frac{\dot{\mathbf{r}}' - \dot{\mathbf{r}}}{\|\mathbf{r}' - \mathbf{r}\|} + \left(\mathbf{n} \cdot \frac{\mathbf{\Omega} + \mathbf{\Omega}'}{2} \right) \mathbf{n}. \end{aligned} \tag{4}$$

k_s is the shear stiffness, $\mathbf{v}_s$ is the relative shear velocity, and the spin vector $\mathbf{\Omega}^C$ defines the rotation of the contact pair in the reference frame [such that in a rigid rotation the contact forces defined by Eq. (4) corotate].

In addition, the shear force remains bounded by Coulomb's friction, imposing

$$\left\| \mathbf{F}_s^C \right\| \leqslant \mu_m \left\| \mathbf{F}_n^C \right\|, \tag{5}$$

with μ_m being the coefficient of contact friction. If at any stage the incrementation based on Eq. (4) leads us to violate Coulomb's inequality, then the magnitude of $\mathbf{F}_s^C$ is decreased accordingly.

C. Fluid model

The fluid has two distinct contributions to the forces on the particles: pairwise lubrication forces opposed to the relative motion of adjacent particles and seepage forces arising whenever the fluid and the solid phase do not comove. The first contribution is detailed in this section; the second one is only outlined. The approach follows Ref. [20] overall, yet it differs quantitatively by the relative magnitude of the two force contributions.

The set of particle pairs for which lubrication force torques are calculated is the set of nearest neighbors as defined by an underlying Delaunay triangulation of the sphere packing. The triangulation is updated during the deformation process so that at any point in time a branch in the Delaunay graph corresponds to a lubricated interaction. It leads to a maximum distance of interaction of the order of $1.5a$. The lubrication force torques for one pair are defined by decomposing the relative motion in four elementary modes: normal displacement, shear displacement, rolling, and twisting. For two particles, the forces are given by the following expressions (respectively, the normal force,

the shear force, the rolling torque, and the twisting torque [20,23]):

$$\mathbf{F}_n^L = \frac{3}{2}\pi\eta_f\frac{a^2}{h}\mathbf{v}_n, \tag{6}$$

$$\mathbf{F}_s^L = \frac{\pi\eta_f}{2}\left[-2a + (2a+h)\ln\left(\frac{2a+h}{h}\right)\right]\mathbf{v}_s, \tag{7}$$

$$\mathbf{T}_r^L = \pi\eta a^3\left(\frac{3}{2} + \frac{63}{500}\frac{h}{a}\right)\ln\left(\frac{a}{h}\right)\omega\mathbf{n}, \tag{8}$$

$$\mathbf{T}_t^L = \pi\eta_f a^2 h\ln\frac{a}{h}(\omega\cdot\mathbf{n})\mathbf{n}, \tag{9}$$

where η_f is the fluid viscosity, h is the gap between particles, $\mathbf{v}_n = \dot{u}_n\mathbf{n}$ is the relative normal velocity, and $\omega = \mathbf{\Omega}' - \mathbf{\Omega}$ is the relative rotational velocity.

A certain roughness $\varepsilon = \epsilon a$ is introduced as a difference between u_n and h. The gap considered for the lubrication is $h = u_n + \varepsilon$, such that solid contact and lubrication effects play concurrently as soon as $h < \varepsilon$.

In this set of equations, the forces are based on the work of Frankel and Acrivos [24,25], whereas torques are based on that of Jeffrey and Onishi [26,27]. The reason for this choice is developed by Marzougui *et al.* [20]. The total lubrication forces and torque applied on particle k and k' are

$$\mathbf{F}_k^L = -\mathbf{F}_{k'}^L = \mathbf{F}_n^L + \mathbf{F}_s^L, \tag{10}$$

$$\mathbf{T}_k^L = \left(a_k + \frac{u_n}{2}\right)\mathbf{F}_s^L\times\mathbf{n} + \mathbf{T}_r^L + \mathbf{T}_t^L, \tag{11}$$

$$\mathbf{T}_{k'}^L = \left(a_k' + \frac{u_n}{2}\right)\mathbf{F}_s^L\times\mathbf{n} - \mathbf{T}_r^L - \mathbf{T}_t^L. \tag{12}$$

The above expressions of lubrication forces and torques are frame invariant and, since they satisfy Newton's third law (of action-reaction), their net contribution to the total force on the solid phase is null.

Conversely, the contribution by the seepage forces is the one which reflects the viscous resistance to differential velocity and net interaction forces between the solid and the fluid phases. Herein this contribution is obtained by integrating an upscaled form of the continuity equation, using the pore-scale finite volume scheme defined by Chareyre *et al.* [28] and Catalano *et al.* [29]. The volume elements—so-called pores—are the tetrahedra of the underlying Delaunay triangulation. The assumptions of the model are that the fluid is strictly incompressible and Newtonian and that the flow is Stokesian. On this basis, the pressure field in the fluid is obtained for the entire problem by solving a linear system of equations dependent on particles' positions and velocities. The seepage forces are then deduced from the pore pressure field and integrated through the law of motion [Eq. (1)]. The pore pressure as well as the resulting forces are updated at every time iteration to capture the strong two way couplings (see Ref. [29]).

The contribution of the seepage forces is evident in various processes such as sedimentation, consolidation, and migration of particles within a flow. It might be argued that such forces are irrelevant to sheared suspensions at steady state, on the basis that both phases essentially comove. While this might be true when averaging the motion of each phase on a sufficiently long time interval, it is not necessarily true when considering instantaneous velocities. Instead, the velocity fluctuations at the particle scale necessarily lead to converging particle velocities in some places, balanced by diverging velocities in other places. This in turns leads to transfers of fluid between mesoscale domains and to seepage forces. The results of Marzougui *et al.* [20] suggested that the dissipation by such internal transfers is negligibly small. However, the seepage forces therein were underestimated by orders of magnitude. A reassessment of the claim with correct orders of magnitude is thus offered in Sec. III A.

D. Numerical details

The suspension is represented by a three-dimensional (3D) biperiodic packing made of $N = 5000$ spheres, of average radius a. The problem is periodic in the shear and vorticity directions and nonperiodic in the third (normal) direction. The dimensions of the simulation cell are $30a \times 30a$ in the periodic directions. The initial state for the shear flow is obtained by compressing in the normal direction a very dilute suspension made of the N spheres placed randomly, in a box of size $30a \times 30a \times 120a$. Once the desired solid fraction is reached, the shear is started.

In the normal direction, the suspension is bounded by additional layers of spheres of the same size which play the role of rough and rigid plates (Fig. 2). The shear is imposed by assigning to the plates opposite velocities in the shear direction. In the normal direction, two sorts of boundary condition are used during shear. The distance between the plates is controlled in order to impose, either a constant solid fraction (distance kept constant) or a constant normal granular stress. In the latter case, the distance is servocontrolled using proportional–integral–derivative regulation to keep the stress close to the target value, and the relative velocity is updated to keep the shear rate constant as the distance changes. The evaluation of granular stress is detailed in the last paragraph of this section. For the pore fluid, the plates are defined as impervious in the case of constant solid fraction and, conversely, a condition of null pore pressure is imposed in the case of imposed granular stress. In both cases, the fluid is assumed to comove with the plates (no slip).

The radii of the spheres are set randomly according to a Gaussian distribution with a standard deviation of 5%. This small polydispersity prevents the system from crystallizing. We have paid a special attention to this issue. For all the results presented in this work, the autocorrelation function of spheres positions do not exhibit any signature of long-range ordering. We also verified that the time-averaged strain rate is homogeneous. For $I_v < 10^{-4}$, however, we observed layering and strain localization close to the walls. In this paper, we restrict the range of viscous numbers above this limit.

All the monitored quantities exhibit a transient regime before reaching the steady state. Since fluctuations can usually be observed even at steady state, we compute time averages of the relevant quantities, with a sufficiently long period so that the uncertainty on the average is less than a few percent.

The two types of boundary conditions in the normal direction (constant volume and constant normal stress) are not exactly equivalent since, for the constant volume case, the confining pressure is allowed to fluctuate, while for the constant pressure it is the solid fraction which fluctuates. However, for the results reported in this paper, we checked that this difference does not lead to significant changes in the observed behavior. In fact, similar to the experimental case, it is more convenient to impose pressure at low viscous numbers. Indeed, in this concentrated regime, small changes of solid fraction have important consequences due to the vicinity of the jamming point. Thus, imposing both the global shear rate and the total pressure allows to study suspensions closer to jamming (vanishing viscous number).

The volume-averaged stress in the system is calculated based on the so-called *virial stress* expression for a particulate system: $\sigma = \langle \mathbf{f} \otimes \mathbf{l} \rangle - m \langle \mathbf{v} \otimes \mathbf{v} \rangle$. The first term on the right-hand side is the volume-averaged outer product of the interaction force $\mathbf{f}$ between two particles and the branch vector $\mathbf{l}$ connecting their reference points. $\mathbf{v}$ is the velocity fluctuation, i.e., the deviation of individual particle velocity from the macroscopic, average, velocity field. The second term, also called "inertial stress," is always negligible in our simulations, as we stay in the viscous regime. Replacing the total interaction force by distinct contributions from contact ($\mathbf{F}_C$) and lubrication ($\mathbf{F}_L$) yields two stress tensors associated to contacts and lubrication, respectively, $\sigma_c = \langle \mathbf{F}_C \otimes \mathbf{l} \rangle$ and $\sigma_L = \langle \mathbf{F}_L \otimes \mathbf{l} \rangle$. The viscosity can be then calculated, taking the xy component of stress tensor: $\eta = \frac{\sigma_{xy}}{\dot{\gamma}}$. From the stress decomposition given above, it is possible to distinguish the contributions of contact and lubrication forces to the effective viscosity.

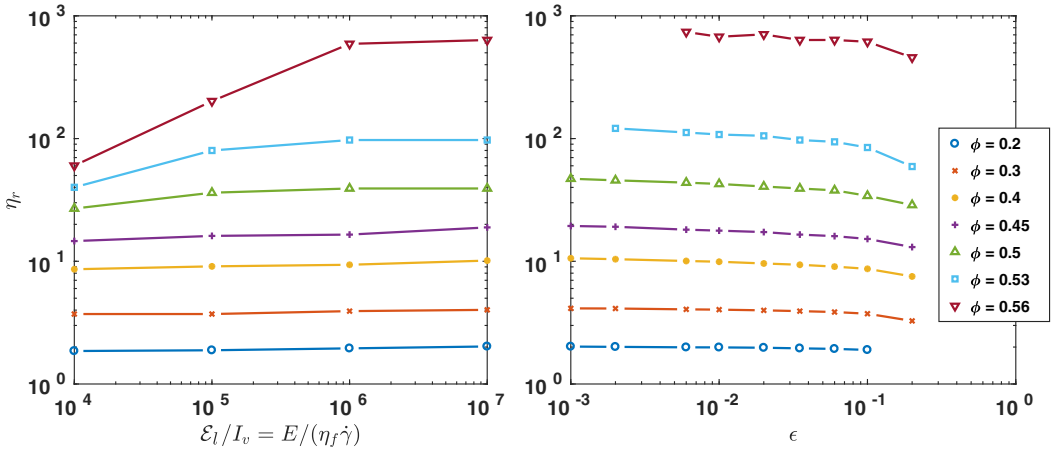

FIG. 1. Sensitivity analysis of the (left) contact stiffness and (right) roughness on the relative viscosity, for various solid fractions. Simulations at imposed solid fraction, $N = 5000$, $\mu_m = 0.4$, $\epsilon = 0.02$ (for stiffness), and $k/(\eta_f\dot{\gamma}) = 10^7$ (for roughness).

E. Parameters and asymptotic regimes

Both the relative viscosity η_r and the macroscopic friction coefficient μ are normalized forms of the shear stress, which is considered here as a response of the system. They are redundant in that sense yet both of them are used hereafter since η is classical in the literature and predicted as a function of ϕ by a number of models, while μ enables better insight into the granular contribution to stresses.

Several dimensionless numbers characterize the flow of non-Brownian suspensions and controls the shear stress. The viscous number, defined as $I_v = \eta_f\dot{\gamma}/P_p$, is the main parameter which has been varied in this work, from 10^{-4} to 10. It is closely related to the solid fraction ϕ, such that imposing one of ϕ or I_v gives the other one as a result. The elastic number $\mathcal{E}_l = E/P_p$ measures the magnitude of sphere deformation by forces from solid contacts. E defines normal contact stiffness k_n according to $k_n = a\,E$. The particulate Stokes number $\mathrm{St}_p = \rho a^2\dot{\gamma}/\eta_f$ defines the ratio of inertial to viscous forces. In addition to these dimensionless numbers, the coefficient of contact friction μ_m and the particle roughness ϵ are material parameters of the problem.

Only I_v and μ_m have been varied systematically, but we checked that the others were small enough (Stokes number and roughness) or high enough (elastic number) to reach an asymptotic regime of inertialess suspensions of rigid and smooth particles. This analysis is detailed in this section.

Unless stated otherwise for sensitivity analysis (see below), all the simulations were done with roughness $\epsilon = 2 \times 10^{-2}$, elastic number $\mathcal{E}_l$ ranges from 10^3 to 10^8, and particle Stokes number ranges from 10^{-5} to 10^{-2}. For sufficiently high elastic numbers and low Stokes numbers, one could expect an asymptotic regime which depends neither on elasticity nor on inertia, and which correspond to the case of rigid spheres in a Stokesian flow. Despite the high and low values of $\mathcal{E}_l$ and St, respectively, it is worth checking this limit. For the elastic limit, we varied the contact stiffness of the spheres. As shown in Fig, 1, the relative viscosity seem to be close to an asymptotic value for dimensionless stiffness $[E/(\eta_f\dot{\gamma})]$ greater than 10^6. For approaching the noninertial limit, we proceeded differently. We computed systematically the contribution of inertia to the global shear stress. It is generally negligible and even for the highest velocities, it remains below 1%. Therefore, all the results reported in the following can be considered in the viscous and rigid limit.

Finally, it is also interesting to test the sensitivity of the simulation results with respect to the particle roughness. Let us recall that the latter used in the model defines the solid contact between

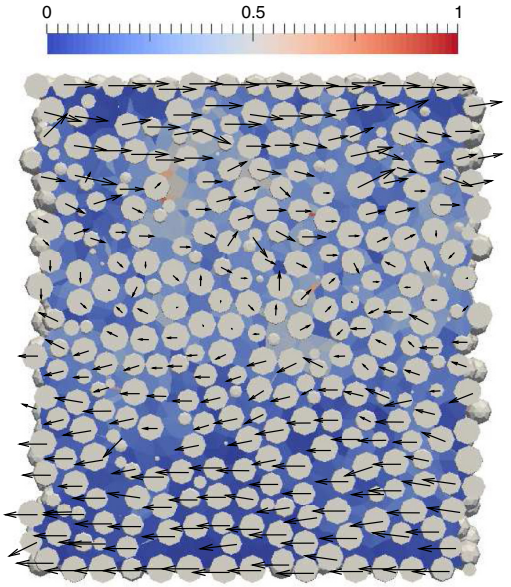

FIG. 2. Snapshot of a slice of the system, normal to the vorticity direction. The arrows indicate the particle velocities, and the colors correspond to the magnitude of the pressure gradient, normalized by the global confining pressure (see color bar). This example has been obtained at $I_v = 10^{-2}$ for $\mu_m = 0.3$.

two spheres; it occurs when the gap is less than roughness. This prevents the lubrication forces from diverging. We varied the roughness between 3×10^{-3} and 2×10^{-1}. The results are shown in Fig. 1. As the relative viscosity reaches a plateau for roughness of less than 4×10^{-2}, we can conclude that there exists an asymptotic limit. In the following, the roughness is fixed at 2×10^{-2}.

III. RESULTS

A. Role of pore pressure

Let us first focus on the role of pore pressure. As explained in the previous section, the model incorporates feedback from fluid pressure to particle motion. However, since this step is computationally costly, it is practically interesting to know whether pore pressure effects can be neglected at least in steady-state shear configurations: It is worth noting that they are very important in transient regimes accompanied by changes in solid fraction.

Figure 2 displays a typical slice of the system, normal to the vorticity direction, at steady state. Rather than the pressure field, we have represented the magnitude of the pressure gradient. The latter is indeed of the order of the local viscous stress acting on a particle by seepage effects. The magnitude of pressure gradient is rather heterogeneous, but it appears in the figure that it remains significantly smaller than the total (bulk) shear stress overall. In Fig. 2, it is typically between 10% and 20% of the mean shear stress, exceeding 20% in only a few places. This snapshot is extracted from a movie obtained available as supplementary material [30].

As it does not seem possible to reach a clear conclusion by comparing the magnitude of local pressure gradients with the global shear stress, we compared the bulk viscosity obtained with and without the coupling with pore pressure (that is, excluding seepage forces from the forces contributing to particles motion). The results are displayed in Fig. 3. The viscosity is remarkably similar in both cases. This result holds for the other macroscopic observables (not presented here for the sake of concision), normal pressure or solid fraction.

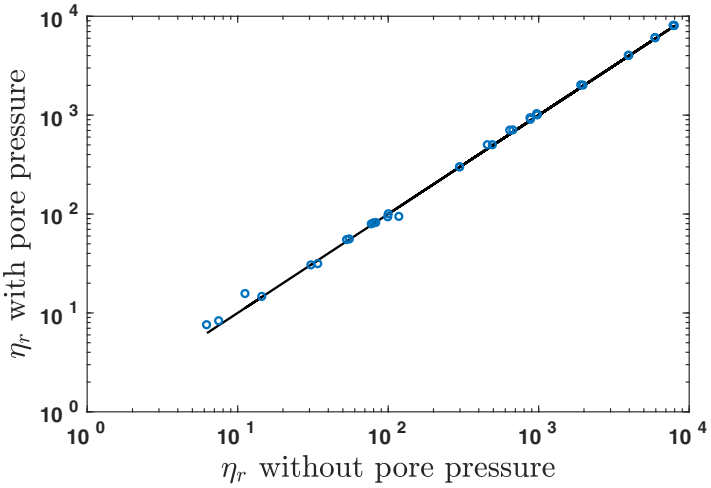

FIG. 3. Comparison of the shear viscosity obtained with and without pore pressure feedback. For this comparison, $\mu_m = 0.3$. The solid line corresponds to equality.

It leads to the conclusion that the effects of pore pressure on macroscopic quantities is negligibly small at steady state, as suggested in Ref. [20] (on a weaker basis). A similar conclusion was also reached recently by Gallier and coworkers [31], who studied the impact of long-range hydrodynamic interactions and found no significant effect. Note that pore pressure may have some effects locally, but their study falls out of the scope of the present work. Since the coupling with the pressure field can be neglected, we performed the systematic simulations presented in the following without this coupling, which saves about 80% of computing time.

B. Shear viscosity

Figure 4 compiles various results, giving reduced viscosity $\eta_r = \eta/\eta_f$ as a function of solid fraction, after earlier papers as well as the present study. The results were obtained either by fixing the solid fraction or the normal confining pressure, with viscous number ranging from 10^{-4} to 10, and for various contact friction μ_m. We find that η_r increases with μ_m, in agreement with previous work [9,10]. The viscosity also seems to diverge at a solid fraction ϕ_m which depends on μ_m.

At this stage, it is worth comparing these data with previous experimental and numerical results. As shown in Fig. 4, the experimental results of Boyer *et al.* [11] are in very good agreement with the data obtained for $\mu_m \simeq 0.5$. More precisely, the correlation proposed by Boyer *et al.* [11] falls in between the data obtained for $\mu_m = 0.36$ and $\mu_m = 0.57$. As the friction coefficient remains to be measured for the systems tested in that work, we can only mention that this order of magnitude is typical of many materials [33]. As most of the experimental data available in the literature are rather similar to those of Boyer *et al.* [11], and as we are not aware of results on simple systems for which the friction coefficient is determined independently, we can only conclude that our results seem to be compatible with experimental data. Concerning simulations results, we compare in Fig. 4 our results to two sets of data obtained with similar models, i.e., with models that consider both contact forces and lubrication forces. The approach of Mari *et al.* [9] is very similar to ours and two extreme cases have been considered: a frictionless one, for which $\mu_m = 0$, and a infinite friction coefficient. Although a small discrepancy is observed for the frictionless system, a very good agreement is obtained in the frictional limit. The comparison with the results reported in Gallier *et al.* [10] is also interesting, because they were obtained with a full resolution of the Stokes equation. In the common range of solid fraction $\phi < 0.45$, the comparison is excellent. This strengthens the conclusion of the

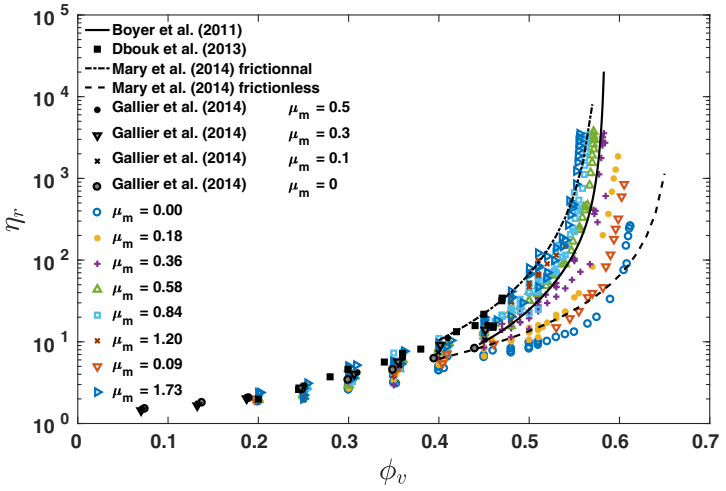

FIG. 4. Relative viscosity as a function of solid fraction, for various microscopic friction coeficients (see legend). Present data (open symbols) are compared to experimental results of Boyer *et al.* [11] and Dbouk *et al.* [32] and numerical results of Mari *et al.* [9] and Gallier *et al.* [10].

previous section: Down to $\phi \simeq 0.2$, neglecting long range viscous forces is a valid approximation. Lubrication forces seem to be sufficient to account quantitatively for the relative viscosity.

C. Confining pressure and frictional rheology

As explained in the introduction, one needs an additional constitutive relation to fully describe the interplay between shear stress, confining pressure, and solid fraction. We follow in this section the approach of Boyer *et al.* [11], who introduced by analogy with granular materials the effective friction coefficient $\mu = \tau/P_p$ and the viscous number $I_v = \eta_f \dot{\gamma}/P_p$. In Figs. 5 and 6, we represent the dependencies $\mu = \mu(I_v)$ and $\phi = \phi(I_v)$ respectively, based on the same dataset as in previous section.

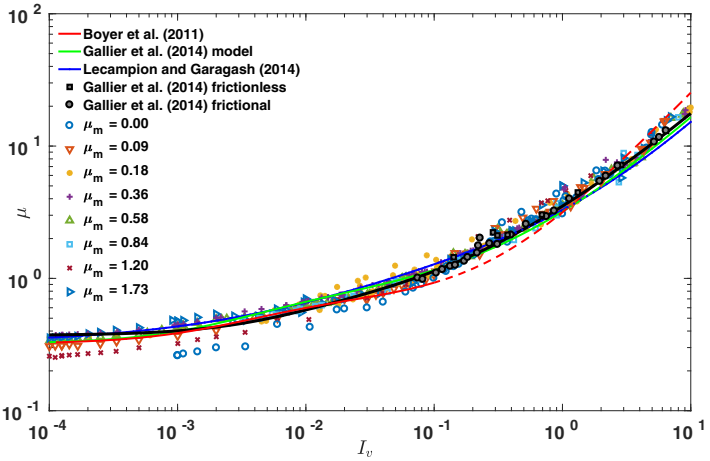

FIG. 5. Effective friction coefficient $\mu = \tau/P_p$ as a function of I_v, for various microscopic friction coefficients μ_m, as indicated in the legend. Data from Refs. [10,11] are superimposed for comparison.

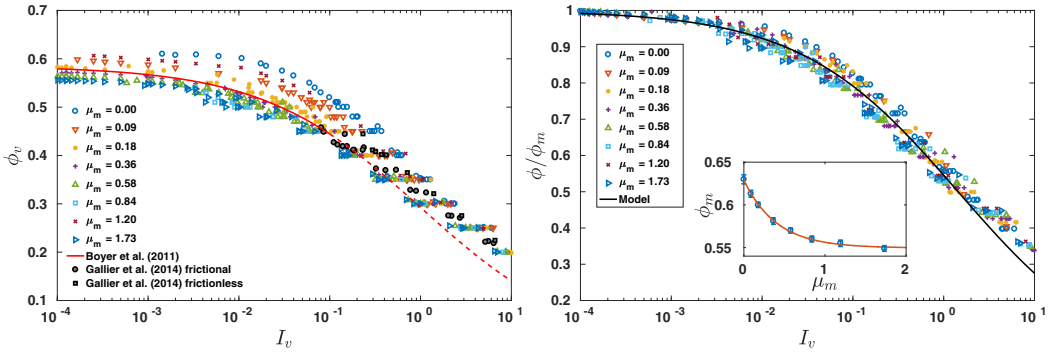

FIG. 6. (a) Solid fraction as a function of the viscous number for various value of μ_m, as indicated in the legend. The solid line represents the correlation proposed in Boyer *et al.* [11], $\phi = \phi_m/(1 + I_v^{0.5})$, which accounts well for the experimental data, for $I_v < 0.1$. The dashed line is simply the extrapolation of this correlation at higher viscous numbers, where no experimental data are available. (b) Same data, but the solid fraction is normalized by its asymptotic value ϕ_m at low I_v. The solid line represents the correlation $1/(1 + I_v^{0.5})$. In insert are shown the different values of ϕ_m as a function of the microscopic friction coefficient. The data are fitted by an exponential function, which accounts well for the data, and displayed in Eq. (13).

In Fig. 5, the results are in very good agreement with earlier simulations as well as experiments. Interestingly, the experimental results of Boyer *et al.* [11] have been obtained in the concentrated regime (I_v between 10^{-4} and 10^{-1}) and the numerical results of Ref. [10] in a more dilute one (I_v between 10^{-1} and 10). Our results cover the whole range of viscous numbers and thus confirm both sets of data.

Strikingly, and in contrast to the shear viscosity, $\mu(I_v)$ is only weakly dependent on contact friction. Exceptions are only found at low I_v; in that case, substantial deviations are obtained for the less frictional systems. The effective friction coefficient is slightly lower in these cases: The asymptotic value at $I_v \to 0$ is about 0.37 for frictional spheres and seems to be of the order of 0.1 for the frictionless one. This last value is in good agreement with the quasistatic limit of frictionless granular materials [34]. For $I_v \gtrsim 10^{-1}$, all results—even for the frictionless case—collapse on a master curve, in good agreement with the numerical results reported in Ref. [10]. For the shear viscosity, similarly, the experimental data of Ref. [11] is close to the results with $\mu_m \simeq 0.5$.

In Fig. 6, the constitutive laws $\phi(I_v)$ deduced from the simulation results are presented. In contrast with the weak dependence of μ on μ_m, discussed above, there is a noticeable decrease of $\phi(I_v)$ at increasing μ_m. This is consistent with the fact that the maximal solid fraction at which the viscosity diverges (see Fig. 4) increases when decreasing μ_m. Comparison with existing data is again excellent on the whole range of I_v tested. In the dilute regime, a quantitative agreement is found with the simulations of Ref. [10]. In the concentrated regime, our results with $\mu_m \simeq 0.45$ match the experimental data. In order to simplify the overall description, we test here the idea that the $\phi(I_v)$ follows a master curve when rescaled by the maximal solid fraction ϕ_m. This is made in Fig. 6. From the very good collapse of the data, we can conclude that there seems to be a universal relation $\phi/\phi_m = f(I_v)$, independent of the value of μ_m. ϕ_m decreases with microscopic friction coefficient, from $\phi_m = 0.63$ for frictionless particles down to $\phi_m = 0.55$. This last value seems to be close to the asymptotic one for $\mu_m \to \infty$. For practical purposes, we propose the following empirical relation between ϕ_m and μ_m:

$$\phi_m = 0.6301 - 0.0794\left[1 - \exp\left(-\frac{\mu_m}{0.4032}\right)\right]. \tag{13}$$

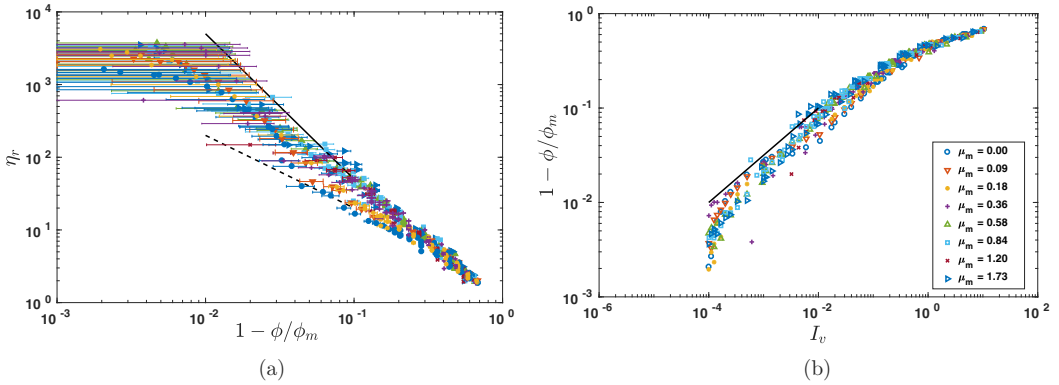

FIG. 7. (a) Reduced viscosity (same data as in Fig. 4), plotted as a function of the distance to jamming, $1-\phi/\phi_m$. Solid and dashed lines represent power law functions of exponents -2 and -1, respectively. (b) $1-\phi/\phi_m$, plotted vs the viscous number I_v for the whole range of μ_m tested. The solid line represents $I_v^{1/2}$.

Let us comment on the values of ϕ_m, as it is not simple to define them unambiguously. We tested several methods: fitting with the empirical relation proposed in Ref. [11] [$\phi = \phi_m/(1+I_v^{0.5})$], manual adjustment of the master curve, average value of ϕ at low I_v. Finally, we chose to define ϕ_m as the value leading to a single power law when $1-\phi/\phi_m$ is plotted as a function of I_v at small I_v. All the methods lead to very similar values. Their variability let us estimate the uncertainty on ϕ_m determination, which is around 0.01 (see the error bars in the insert of Fig. 6).

Note that another functional form for $\phi_m = \phi_m(\mu_m)$ was proposed in Singh *et al.* [35]. Its main difference with Eq. (13) is that $\frac{d\phi_m}{d\mu_m}(\mu_m = 0^+) = 0$ in the former, which is not compatible with our data.

It is worth noting finally that the sensitivity to contact friction, more pronounced for the solid fraction than for the macroscopic friction, is a common feature of both suspensions and dry granular flow. The latter case was reported by Aboul-Hosn *et al.* [36], for instance (Fig. 5 therein).

D. Critical scaling near jamming

One of the recurrent questions in the literature concerns the exponents governing the divergence of the viscosity when approaching the maximal solid fraction. Although most authors report that $\eta \sim (\phi-\phi_m)^{-\alpha}$, with $\alpha \simeq 2$, some theoretical arguments are in favor of a different scaling relation between frictional and frictionless particles [18]. Note that, as pointed out by several authors (see, for example, Ref. [9]), the determination of the exponents is nontrivial. In Fig. 7, we replot the viscosity data in a log-log axis system, and as a function of $(1-\phi/\phi_m)$. As explained above, it is difficult to define ϕ_m very accurately. This uncertainty leads to the large error bars displayed in Fig. 7 when approaching ϕ_m. It prevents us from reaching a precise conclusion on the scaling exponent. For $1-\phi/\phi_m \gtrsim 0.1$, the α exponent is clearly close to 2. For lower values, it is between 1 and 2. We note that for the frictionless system, the slope seems to be closer to 1 than to 2 and smaller than that of frictional cases, in agreement with previous reports [31].

Alternatively, we can examine the scaling of $1-\phi/\phi_m$ when decreasing I_v. Since $\eta_r = \mu/I_v$ and assuming that μ tends to a constant value when $I_v \to 0$, $(1-\phi/\phi_m)$ should scale as $I_v^{1/\alpha}$. Strikingly, as shown in Fig. 7, the data exhibit a nice collapse on a power law of exponent 0.5. Note that this scaling relation is observed across three orders of magnitude ($10^{-4} < I_v < 10^{-1}$). The fact that the scaling relation is less clear when considering the viscosity can be understood on the basis that μ has not reach the quasistatic value and keeps decreasing when decreasing I_v down to 10^{-4}. Determining the divergence exponent for viscosity from the simulations would thus require to decrease I_v even below 10^{-4} and to define ϕ_m more accurately.

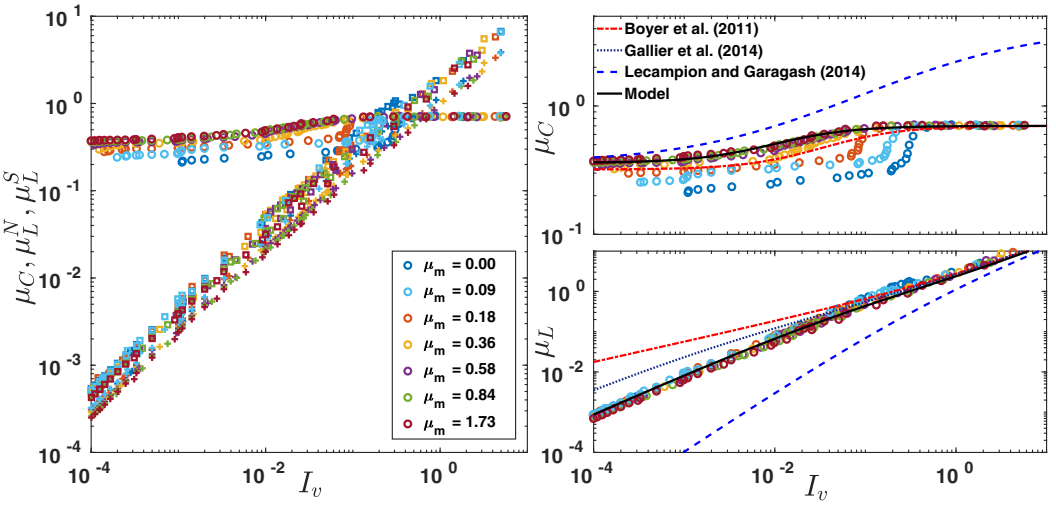

FIG. 8. Contact and lubrication contribution to the effective friction coefficient. (Left) All the components (circles for contact contribution, squares for normal lubrication contribution, and crosses for shear lubrication contribution) are plotted as a function of I_v. (Right) Magnified plot of (top) the contact contribution and (bottom) the sum of lubrication contribution ($\mu_L = \mu_L^N + \mu_L^S$). Discontinuous lines are models proposed by different authors. Contact contribution proposed by Gallier *et al.* [10] is the same as that proposed by Boyer *et al.* [11]. Solid lines represents the model proposed in Eqs. (14) and (15).

E. Stress decomposition and phenomenological relations

We now take advantage of the simulation results to discuss the role of contact forces. We propose, as in Refs. [9–11,18,20,37], to analyze the contributions to the total shear stress from contact forces and lubrication forces, respectively.

As seen in Fig. 8, the fraction of μ attributed to contact forces, noted μ_C, is slowly increasing with I_v, but remains in the range 0.1–0.7. In contrast, the viscous contribution μ_L is increasing almost linearly. As a consequence, the total shear stress is dominated by lubrication forces at high viscous number, and more precisely for $I_v > 0.1$. This crossover does not depend significantly on the value of μ_m. For lower values of I_v, the contact forces are dominant. It is interesting to comment on the crossover in terms of solid fraction, as many experiments are conducted at fixed solid fraction. As detailed in the previous sections, when varying the microscopic friction coefficient, the solid fraction $\phi(I_v)$ is modified, and we have shown that a master curve could be obtained when ϕ is normalized by the maximal solid fraction ϕ_m. Therefore, the crossover observed at $I_v \simeq 0.1$ between a contact dominated rheology and a lubrication dominated one corresponds to a value of $\phi/\phi_m \simeq 0.77$. Using the $\phi_m(\mu_m)$ dependency displayed in Fig. 6(b), we obtain for a frictionless system a crossover solid fraction of $\phi \simeq 0.48$; when the friction coefficient is very high, the crossover is reduced to $\phi \simeq 0.42$. This range is compatible with the range leading to discontinuous shear thickening in Ref. [8].

The contribution of normal and tangential lubrication forces follow very similar trends. The tangential forces contribute to approximately one third of the total lubrication stress in all cases. Though smaller than the contribution of normal forces, it is not negligible.

The stress decomposition discussed above also allows us to test and revisit the phenomenological expressions that have been proposed in the literature on $\mu(I_v)$ rheology. To our knowledge, three different expressions have been proposed. The first one, by Boyer *et al.* [11], is based on experimental data and therefore without any data from the stress decomposition. The second one was proposed in Ref. [10], based on numerical results obtained for $I_v > 0.1$ and thus restricted to the lubrication-dominated regime. Finally, the last one was proposed by Lecampion and Garagash [37], without data support, but with the objective of removing the nonmonotonicity of the $d\phi/d\mu$

with respect to ϕ, which exists in Boyer's correlation. These three phenomenological models are detailed in the Appendix. We note that although these three correlations lead to rather similar $\mu(I_v)$ relations (see Fig. 5), their decompositions in terms of viscous and contact contributions are rather different and their asymptotic scaling differ. The differences between the hydrodynamic contributions are evident in the concentrated regime where this contribution is negligible, and conversely the differences between contact contributions are more visible in dilute regime. We have plotted in Fig. 8 the decompositions of all three models together with the data reported in this article. There is an evident mismatch between the expressions from Lecampion and Garagash [37] and our results. The hydrodynamic contribution proposed in Boyer *et al.* [11] fails to predict the asymptotic scaling at low I_v: it scales as $\mu_h \propto I_v^{1/2}$, whereas we observe $\mu_h \propto I_v$ in the concentrated regime. Finally, the expression from Gallier *et al.* [10] is in quantitative agreement for $I_v > 10^{-1}$ but it overestimates μ_L at lower values (a regime unexplored in that work). Nonetheless, it exhibits a correct linear scaling as $I_v \to 0$. The contact contribution is relatively well captured by the expression of Boyer *et al.* [11], which was kept unchanged by Gallier *et al.* [10].

To sum up, the expressions proposed by Gallier *et al.* [10] are in qualitative agreement with our data. In order to improve the quantitative agreement, however, we suggest a change in the empirical coefficients. The model we propose finally reads

$$\mu = \underbrace{\mu_1 + \frac{\mu_2 - \mu_1}{1 + I_0/I_v}}_{\mu_c} + \underbrace{I_v \left(1 - \phi_m \frac{1}{1 + I_v^{\frac{1}{2}}}\right)^{-[\eta]}}_{\mu_h} \tag{14}$$

$$\frac{\phi}{\phi_m} = \frac{1}{1 + I_v^{\frac{1}{2}}} \tag{15}$$

with $\mu_1 = 0.36$, $\mu_2 = 0.7$, $I_0 = 0.0133$, $[\eta] = 5/2$. As shown in Fig. 8, this model is in very good agreement with the data in the whole range of viscous number studied and for both lubrication and contact components of the total shear stress. Complemented by the phenomenological relation relating ϕ_m and μ_m [see Eq. (13)], it allows us to predict accurately the shear viscosity and the solid fraction of a suspension made of rigid spheres of known microscopic friction coefficient.

Eliminating the viscous number in Eqs. (14) and (15) leads to the following expression for the shear viscosity as a function of the solid fraction:

$$\eta_r = \frac{\mu_1}{(\phi_m/\phi - 1)^2} + \frac{\mu_2 - \mu_1}{(\phi_m/\phi - 1)^2 + I_0} + (1 - \phi)^{-5/2}. \tag{16}$$

The first two terms are originated from contact forces and the last one from lubrication. Interestingly, this expression is asymptotically equivalent to Einstein relation [1] at low ϕ, as $\eta_r = 1 + \frac{5}{2}\phi + O(\phi^2)$. Moreover, it is also asymptotically equivalent to the Krieger-Dougherty form when ϕ is approaching ϕ_m, as $\eta_r \sim \mu_1(1 - \phi/\phi_m)^{-2}$. Note that the -2 exponent is compatible with most of the data available in the literature.

The above model captures quantitatively the data reported in this article as soon as $\mu_m > 0.36$. For lower values of μ_m, we observe that the macroscopic friction coefficient μ (and consequently the shear viscosity) depends on μ_m through the contact contribution. This is evidenced in Fig. 8 (bottom left). Not only does the value of μ_1 slightly decrease when μ_m is decreased below 0.36, but also the transition toward the asymptotic value μ_2 at high I_v is sharper and shifted to larger I_v value. Looking into detail and in particular at the volume fraction profiles, we noticed that this sharp transition is accompanied by a wall-induced layering of the spheres when decreasing I_v, recalling some of the results of Ref. [38]. In contrast, when the transition is smooth for $\mu_m \geqslant 0.36$, the whole domain remains disordered in the range of I_v investigated. Because of this layering, it seems meaningless to adapt the correlation proposed in Eq. (14) for the weakly frictional systems. Describing or removing the layering in these ones asks for additional dedicated work, as it is likely that this phenomenon

depends on the confinement and on wall details. Let us finally note that the condition $\mu_m > 0.36$ for the frictional limit is satisfied by a large range of materials.

IV. CONCLUSION

A systematic study of sheared suspensions of frictional and frictionless rigid spheres has been carried out by numerical simulations, in a large range of viscous numbers. The good quantitative agreement between the numerical results and available experimental data suggests that the main two components of the model considered here, i.e., lubrication and contact forces, are sufficient to explain the rheology of these systems. A more detailed analysis showed that lubrication forces dominate for $I_v > 10^{-1}$, i.e., for $\phi/\phi_m < 0.77$, while contact forces give the main contribution to shear stress otherwise. Viscosity, solid fraction and viscous number are linked together by two constitutive laws, which only depend on the microscopic friction coefficient. Among the results reported in this article, we should empasize that in a large range of parameters viscosity is defined uniquely as a function of I_v, independent of contact friction. Exceptions to this rule are found only for weakly frictional contacts at low I_v. Moreover, normalizing the solid fraction by the upper bound $\phi_m = \phi$ ($I_v = 0$) defined for a given contact friction leads to a master curve as a function of I_v only. In other words, even when contact forces between the particles dominate the flow, changing the friction between particles only affects the maximal solid fraction at which the viscosity diverges.

A complete set of constitutive relations has been offered, which fits the numerical data accurately across five orders of magnitude of I_v. This constitutive model is close to previous ones in terms of total shear stress yet the decomposition in terms of lubrication and contact forces differs from previous ones and is consistent with presented data. As it asymptotically matches the standard Einstein relation at low ϕ and Krieger-Dougherty law at high ϕ (with a -2 divergence exponent), we believe it could be extrapolated to an even larger range of I_v.

Apart from these main results, let us also highlight that we have validated the fact that the coupling with pore pressure has negligible consequences at steady state, and that long-range hydrodynamic interactions are not relevant down to solid fraction of 0.2. Besides, the results are very sensitive neither to the particle roughness (between 10^{-3} and 10^{-1}) nor to the particle stiffness. The transition toward the limit of ultrasmooth particles where contact between particles do not theoretically exists remains to be investigated. Importantly, even frictionless particles fall well in the picture depicted above and are dominated at low I_v by contact forces, although one should adapt slightly the master curves.

ACKNOWLEDGMENTS

The authors wish to thank S. Gallier, F. Peters, L. Lobry, O. Pouliquen, E. Lemaire, and E. Guazzeli for fruitful discussion. They acknowledge Universitè Grenoble Alpes for financial support. 3SR and LRP are members of Labex Tec21 and LRP of Institut Carnot Polynat. Some of the computations presented in this paper were performed using the CIMENT infrastructure (https://ciment.ujf-grenoble.fr), which is supported by the Rhône-Alpes region (Grant No. CPER07_13 CIRA, http://www.ci-ra.org).

APPENDIX

We detail below the three correlations that have been proposed in the literature for the $\mu(I_v)$ rheology and that are compared to the simulation data in Figs. 5 and 8.

Boyer *et al.* [11] proposed the following correlation, which accounts well for the experimental data:

$$\mu = \underbrace{\mu_1 + \frac{\mu_2 - \mu_1}{1 + I_0/I_v}}_{\mu_c} + \underbrace{I_v\left(1 + \frac{5}{2}\frac{\phi_m}{I_v^{1/2}}\right)}_{\mu_h} \tag{A1}$$

$$\frac{\phi}{\phi_m} = \frac{1}{1 + I_v^{\frac{1}{2}}}, \tag{A2}$$

with $\mu_1 = 0.32$, $\mu_2 = 0.7$, $I_0 = 0.005$, and $\phi_m = 0.585$.

In the expression proposed by Gallier *et al.* [10], the hydrodynamic component μ_h is modified and the model reads

$$\mu = \underbrace{\mu_1 + \frac{\mu_2 - \mu_1}{1 + I_0/I_v}}_{\mu_c} + \underbrace{I_v\left(1 + \frac{\phi_m}{\phi'_m}\frac{1}{1 + I_v^n}\right)^{-[\eta]\phi'_m}}_{\mu_h} \tag{A3}$$

$$\frac{\phi}{\phi_m} = \frac{1}{1 + I_v^n}, \tag{A4}$$

with $\mu_1 = 0.32$, $\mu_2 = 0.7$, $I_0 = 0.005$, $\phi_m = 0.64$, $\phi'_m = 0.68$, $[\eta] = 2.4$, and $n = 0.4$. These parameters are in good agreement with the numerical results reported in Ref. [10], obtained for $\mu_m = 0.5$ for solid fraction between 0.1 and 0.45.

In their 2014 paper, Lecampion and Garagash [37] proposed to significantly modify the forms of both contact and lubrication contributions to the macroscopic friction coefficient, without changing significantly the sum of the two. The corresponding expression reads

$$\mu = \underbrace{\mu_1 + \frac{\phi_m}{\beta}\left(1 - \frac{\phi}{\phi_m}\right)}_{\mu_c} + \underbrace{I_v\left[1 + \frac{\frac{5}{2}\phi_m + 2}{I_v^{1/2}}\right]\left(1 - \frac{\phi}{\phi_m}\right)^2}_{\mu_h} \tag{A5}$$

$$\frac{\phi}{\phi_m} = \frac{1}{1 + I_v^{1/2}}, \tag{A6}$$

with $\beta = 0.158$, $\mu_1 = 0.3$, and $\phi_m = 0.585$.

[1] A. Einstein, Eine neue bestimmung der moleküldimensionen, Ann. Phys. **324**, 289 (1906).

[2] G. Batchelor and J. Green, The determination of the bulk stress in a suspension of spherical particles to order c^2, J. Fluid Mech. **56**, 401 (1972).

[3] F. Gadala-Maria and A. Acrivos, Shear-induced structure in a concentrated suspension of solid spheres, J. Rheol. **24**, 799 (1980).

[4] B. Metzger, P. Pham, and J. E. Butler, Irreversibility and chaos: Role of lubrication interactions in sheared suspensions, Phys. Rev. E **87**, 052304 (2013).

[5] C. Ness and J. Sun, Two-scale evolution during shear reversal in dense suspensions, Phys. Rev. E **93**, 012604 (2016).

[6] F. Peters, G. Ghigliotti, S. Gallier, F. Blanc, E. Lemaire, and L. Lobry, Rheology of non-Brownian suspensions of rough frictional particles under shear reversal: A numerical study, J. Rheol. **60**, 715 (2016).

[7] M. Wyart and M. E. Cates, Discontinuous Shear Thickening Without Inertia in Dense Non-Brownian Suspensions, Phys. Rev. Lett. **112**, 098302 (2014).

[8] R. Seto, R. Mari, J. F. Morris, and M. M. Denn, Discontinuous Shear Thickening of Frictional Hard-Sphere Suspensions, Phys. Rev. Lett. **111**, 218301 (2013).
[9] R. Mari, R. Seto, J. F. Morris, and M. Denn, Shear thickening, frictionless and frictional rheologies in non-Brownian suspensions, J. Rheol. **58**, 1693 (2014).
[10] S. Gallier, E. Lemaire, F. Peters, and L. Lobry, Rheology of sheared suspensions of rough frictional particles, J. Fluid Mech. **757**, 514 (2014).
[11] F. Boyer, É. Guazzelli, and O. Pouliquen, Unifying Suspension and Granular Rheology, Phys. Rev. Lett. **107**, 188301 (2011).
[12] L. Amarsid, J. Y. Delenne, P. Mutabaruka, Y. Monerie, F. Perales, and F. Radjai, Viscoinertial regime of immersed granular flows, Phys. Rev. E **96**, 012901 (2017).
[13] T. Kawasaki and L. Berthier, Discontinuous shear thickening in Brownian suspensions, Phys. Rev. E **98**, 012609 (2018).
[14] C. Ness and J. Sun, Flow regime transitions in dense non-Brownian suspensions: Rheology, microstructural characterization, and constitutive modeling, Phys. Rev. E **91**, 012201 (2015).
[15] A. Boromand, S. Jamali, B. Grove, and J. M. Maia, A generalized frictional and hydrodynamic model of the dynamics and structure of dense colloidal suspensions, J. Rheol. **62**, 905 (2018).
[16] O. Cheal and C. Ness, Rheology of dense granular suspensions under extensional flow, J. Rheol. **62**, 501 (2018).
[17] M. Trulsson, B. Andreotti, and P. Claudin, Transition from the Viscous to Inertial Regime in Dense Suspensions, Phys. Rev. Lett. **109**, 118305 (2012).
[18] M. Trulsson, E. DeGiuli, and M. Wyart, Effect of friction on dense suspension flows of hard particles, Phys. Rev. E **95**, 012605 (2017).
[19] R. N. Chacko, R. Mari, M. E. Cates, and S. M. Fielding, Dynamic Vorticity Banding in Discontinuously Shear Thickening Suspensions, Phys. Rev. Lett. **121**, 108003 (2018).
[20] D. Marzougui, B. Chareyre, and J. Chauchat, Microscopic origin of shear stress in dense fluid-grain mixtures, Granular Matter **17**, 297 (2015).
[21] V. Šmilauer *et al.*, *Yade Documentation*, 2nd ed. (2015), http://yade-dem.org/doc/.
[22] P. Cundall and O. Strack, Discrete numerical-model for granular assemblies, Geotechnique **29**, 47 (1979).
[23] R. Ball and J. R. Melrose, A simulation technique for many spheres in quasi-static motion under frame-invariant pair drag and Brownian forces, Physica A (Amsterdam, Neth.) **247**, 444 (1997).
[24] N. Frankel and A. Acrivos, On the viscosity of a concentrated suspension of solid spheres, Chem. Eng. Sci. **22**, 847 (1967).
[25] B. Van den Brule and R. Jongshaap, Modeling of concentrated suspensions, J. Stat. Phys. **62**, 1225 (1991).
[26] D. Jeffrey and Y. Onishi, The forces and couples acting on two nearly touching spheres in low-Reynolds-number flow, Z. Angew. Math. Phys. **35**, 634 (1984).
[27] D. Jeffrey and Y. Onishi, Calculation of the resistance and mobility functions for two unequal rigid spheres in low-Reynolds-number flow, J. Fluid Mech. **139**, 261 (1984).
[28] B. Chareyre, A. Cortis, E. Catalano, and E. Barthélemy, Pore-scale modeling of viscous flow and induced forces in dense sphere packings, Transport Porous Med. **94**, 595 (2012).
[29] E. Catalano, B. Chareyre, and E. Barthélemy, Pore-scale modeling of fluid-particles interaction and emerging poromechanical effects, Int. J. Numer. Anal. Met. **38**, 51 (2014).
[30] See Supplemental Material at http://link.aps.org/supplemental/10.1103/PhysRevFluids.4.064302 for gradient of fluid pressure in a sheared granular suspension.
[31] S. Gallier, F. Peters, and L. Lobry, Simulations of sheared dense noncolloidal suspensions: Evaluation of the role of long-range hydrodynamics, Phys. Rev. Fluids **3**, 042301 (2018).
[32] T. Dbouk, L. Lobry, and E. Lemaire, Normal stresses in concentrated non-Brownian suspensions, J. Fluid Mech. **715**, 239 (2013).
[33] Faculty of Industrial Design Engineering of Delft University of Technology, IDEMAT database, (2003).
[34] P.-E. Peyneau and J.-N. Roux, Frictionless bead packs have macroscopic friction, but no dilatancy, Phys. Rev. E **78**, 011307 (2008).

[35] A. Singh, R. Mari, M. M. Denn, and J. F. Morris, A constitutive model for simple shear of dense frictional suspensions, J. Rheol. **62**, 457 (2018).
[36] R. A. Hosn, L. Sibille, N. Benahmed, and B. Chareyre, Discrete numerical modeling of loose soil with spherical particles and interparticle rolling friction, Granular Matter **19**, 4 (2017).
[37] B. Lecampion and D. Garagash, Confined flow of suspensions modeled by a frictional rheology, J. Fluid Mech. **759**, 197 (2014).
[38] S. Gallier, E. Lemaire, L. Lobry, and F. Peters, Effect of confinement in wall-bounded non-colloidal suspensions, J. Fluid Mech. **799**, 100 (2016).